Progress In Electromagnetics Research C, Vol. 172, 448–457, 2026

PIER C

(Received 28 May 2026, Accepted 2 July 2026, Scheduled 21 August 2026)

Cross-Entropy Based Optimization for LPDA Antenna Miniaturization

Sudeepa Herath[1, 2, *], Jeevani Jayasinghe[3, 4], Disala Uduwawala[1], and Fabien Ferrero[4]

[1]*Department of Electrical and Electronic Engineering, University of Peradeniya, Sri Lanka*
[2]*Intel Corporation, Penang, Malaysia*
[3]*Department of Electronics, Wayamba University of Sri Lanka, Kuliyapitiya, Sri Lanka*
[4]*Laboratoire d'Electronique, Antennes et Telecommunications (LEAT), Université Côte d'Azur, France*

ABSTRACT: This paper presents the design and experimental validation of a miniaturized Printed Log-Periodic Dipole Array (PLPDA) antenna operating within the 1.3–6.0 GHz frequency range. The objective of this work was to reduce the antenna's overall footprint while preserving its wideband performance. A sequential miniaturization strategy was adopted, employing m-segment fractal geometry for lateral size reduction and Cross-Entropy (CE) optimization for axial compaction. The reference PLPDA, measuring 255 mm × 116 mm, was progressively refined to a final size of 217 mm × 88 mm, achieving an overall footprint reduction of approximately 34%. The simulated and measured results confirmed excellent impedance matching, with S_{11} remaining below -10 dB across the entire operating band and an average gain exceeding 7 dB. These results validate that the proposed CE-optimized m-segment PLPDA successfully achieves substantial miniaturization without degrading bandwidth or radiation performance. The proposed approach offers a practical framework for developing compact, high-performance wideband antennas.

1. INTRODUCTION

A log-periodic dipole array (LPDA) antenna consists of a tapered sequence of dipole elements arranged along a boom, providing stable performance across a broad frequency range through logarithmic periodicity. Although LPDAs were first introduced several decades ago, their design has since been refined and standardized in modern literature, making them a widely adopted wideband solution for applications such as radio astronomy, broadcasting, wireless communication, and spectrum monitoring.

With the growing demand for compact and integrated radio-frequency (RF) systems, research has progressively transitioned from conventional free-space LPDAs to printed LPDA (PLPDA) configurations. The PLPDA offers a streamlined, planar, and easily fabricated structure while maintaining the broadband characteristics of its predecessor. However, despite these advantages, the overall antenna size, both in axial (length) and lateral (width) dimensions, remains a key limitation in applications in which space is constrained. Consequently, recent studies have focused on footprint-reduction strategies, laying the foundation for further investigations into size reduction without compromising wideband performance.

Lateral miniaturization of PLPDAs has been pursued through several geometric modification strategies. Meandered dipole structures [1] reduce width by folding the current path, while modified dipole shapes — including T-top configurations [2], biconical geometries [3], and various tapered profiles [4–7] — achieve width reduction through optimized element shapes and improved current distribution. These approaches demonstrate that careful geometric design can significantly reduce the lateral footprint while maintaining stable impedance characteristics.

Fractal geometries offer an alternative approach to lateral miniaturization by extending current paths and increasing electrical length without enlarging the physical footprint. Various fractal configurations have been investigated for PLPDA applications, including Koch curves [8], Sierpinski triangles [9], Peano curves [10], Hilbert curves [11], and hybrid fractal designs [12–14]. Slot-enhanced fractal implementations [15] further improve miniaturization performance. However, these intricate fractal structures pose fabrication challenges due to increasing complexity with higher iteration orders. The m-segment fractal [16] addresses this limitation by offering designers greater control over the trade-off between miniaturization and fabrication complexity via adjustable segmentation parameters.

While lateral miniaturization has received considerable attention, axial (profile) reduction of PLPDAs remains relatively underexplored. Folded dipole configurations [17] have been investigated for axial compaction but rely on fixed geometries with limited design flexibility. More recently, Pu and Zhang [18] introduced a resonance point optimization (RPO) method that achieves axial size reduction by selectively eliminating redundant dipole elements — retaining approximately 80% of the elements from classical designs while recalculating resonance frequencies and inter-element spacings. Although this approach maintains bandwidth, it results in reduced low-frequency gain. These limitations highlight the need for an adaptive optimization framework capable of exploring the design space dynamically to achieve axial miniaturization without performance degradation.

* Corresponding author: Sudeepa Herath (sudeepa.madushanka.herath@intel.com).

Optimization techniques, such as Particle Swarm Optimization (PSO), Artificial Bee Colony (ABC), and Genetic Algorithms (GA), have been widely applied in antenna design for impedance matching, gain enhancement, and bandwidth improvement [19]. However, their performance may degrade in high-dimensional problems with strongly coupled parameters, often requiring extensive function evaluations to explore complex multimodal design spaces [20]. This challenge is particularly evident in PLPDA miniaturization, where compactness and high-performance requirements — such as wide impedance bandwidth, stable radiation characteristics, and enhanced gain — introduce inherently conflicting design objectives.

Cross-Entropy (CE) optimization [21] adopts a model-based search paradigm in which a probability distribution is iteratively refined using elite samples. By systematically concentrating the sampling distribution around high-performing regions via controlled variance reduction, CE improves convergence stability. As demonstrated in [20], this probabilistic refinement strategy results in significantly fewer function evaluations than population-based methods such as PSO for high-dimensional multimodal problems — for instance, 6,050 versus 38,400 evaluations for a 30-dimensional benchmark, representing approximately a 6-fold reduction. This computational efficiency makes CE particularly suitable for antenna optimization where each design evaluation requires expensive full-wave electromagnetic simulation. Furthermore, CE's elite sampling mechanism improves convergence stability for problems with conflicting objectives — a characteristic directly relevant to PLPDA miniaturization, where bandwidth, gain, and size reduction must be optimized simultaneously.

Despite the extensive research on PLPDA miniaturization, the existing literature predominantly addresses unidirectional size reduction — either lateral or axial dimensions in isolation — with limited attention to achieving simultaneous dual-dimensional compaction. This work addresses this gap by integrating m-segment fractal geometry with Cross-Entropy optimization to achieve concurrent lateral and axial miniaturization of a single-layer PLPDA. The approach offers two key contributions: (1) a dual-dimensional miniaturization framework integrating fabrication-efficient m-segment fractal geometry with CE-optimized spacing, achieving experimental validation of 34% footprint reduction across 1.3–6.0 GHz and (2) application of Cross-Entropy optimization to multi-objective wideband antenna design, demonstrating its capability to balance competing miniaturization and performance objectives through systematic design space exploration. This combination of techniques, substantiated by experimental measurements, distinguishes the present work from prior unidirectional miniaturization approaches and provides a practical framework for compact wideband PLPDA design.

This paper is organized as follows. Section 2 discusses the miniaturization techniques used, namely the m-segment method and CE optimization. Section 3 covers details of the conventional PLPDA design, m-segment PLPDA design, and CE-optimized PLPDA. Section 4 presents the results and discussions, and Section 5 concludes the paper.

2. PLPDA MINIATURIZATION TECHNIQUES

2.1. m-Segment Fractals

Fractals are increasingly used in antenna design for miniaturization because of their space-filling nature. They enable compact designs without degrading performance, making them suitable for modern telecommunication systems.

The m-segment fractal, introduced in [16], is a simple and highly customizable geometry. Unlike conventional fractals based on recursive transformations, the m-segment method divides a line into a fixed number of smaller segments, allowing controlled, flexible structural modification. The number of segments and iteration depth can be adjusted to meet specific design requirements.

The m-segment fractal geometry is characterized by two integer parameters, denoted by m and n. m determines the number of linear segments into which a line of length L is subdivided, and n denotes the iteration count in the fractal generation process.

As highlighted in the foundational literature on m-segment in [16], fractal generation involves two operations: p and q.

$p \rightarrow$ Turn 45° clockwise and travel a distance of $L/m\sqrt{2}$, then turn 90° anticlockwise and travel a distance of $L/m\sqrt{2}$.

$q \rightarrow$ Turn 45° anticlockwise and travel a distance of $L/m\sqrt{2}$, then turn 90° clockwise and travel a distance of $L/m\sqrt{2}$.

If a line segment undergoes operation p (or q), the resulting segment is labeled A (or B). Subsequent iterations are generated based on these labels. The m-segment fractal geometries with $m = 2$ corresponding to the 0th (straight-line), 1st, and 2nd iterations are shown in Fig. 1 [16].

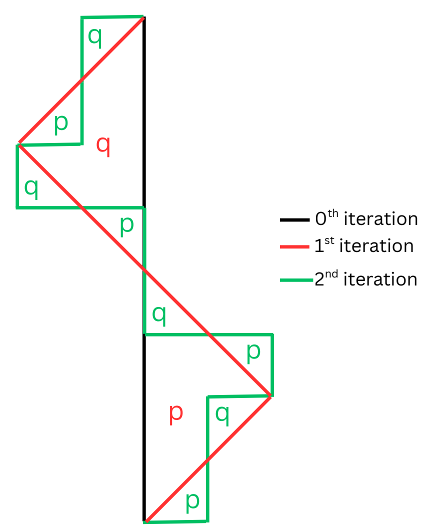

FIGURE 1. m-segment generation with $m = 2$ [16].

As established in our previous work [22], incorporating the m-segment fractal into the dipole structure of a PLPDA effectively reduces the antenna's lateral dimension while maintaining stable bandwidth and gain. In this study, the same m-segment framework is retained for lateral compaction and extended further to enable axial reduction through optimization, as detailed in the following sections.

2.2. Cross Entropy Optimization

The Cross-Entropy (CE) method, introduced by Rubinstein in 1997, is a powerful tool for solving a wide range of optimization problems, including rare-event simulation, combinatorial optimization, and continuous multi-extremal optimization [21]. It is based on Kullback-Leibler minimization and can be applied to various estimation and optimization problems [23]. The CE method has been found advantageous in handling mixed variables and constraints in electromagnetic optimization, leading to improved antenna performance [20].

CE optimization begins by initializing a set of candidate solutions, either randomly or based on informed estimates. These candidates are evaluated against an objective function, and a probabilistic selection process favors those with superior performance. The selected solutions inform the update of algorithm parameters, using cross-entropy to steer the search towards promising regions in the parameter space. This iterative process continues until a termination criterion, such as convergence or a predetermined maximum number of iterations, is achieved.

For a random variable $X = (X_1, X_2, \ldots, X_n)$ with a range of possible values given by the support of X, the Kullback-Leibler (KL) distance between two continuous probability density functions f and g is defined as follows:

$$\begin{aligned} \mathcal{D}(f,g) &= \mathbb{E}_f\left[\log\frac{f(\mathbf{X})}{g(\mathbf{X})}\right] \\ &= \int_{\mathbf{x}\in X} f(\mathbf{x})\log f(\mathbf{x})\,d\mathbf{x} - \int_{\mathbf{x}\in X} f(\mathbf{x})\log g(\mathbf{x})\,d\mathbf{x} \end{aligned} \quad (1)$$

where the expectation of a function with respect to a distribution f is denoted as $\mathbb{E}_f$. The goal of CE optimization is to minimize the KL distance $\mathcal{D}$ between the true distribution f and the optimum distribution g parameterized by θ. Mathematically, this can be denoted as

$$\underset{\theta}{\text{minimize}} - \int_{\mathbf{x}\in X} f(\mathbf{x})\log g(\mathbf{x}|\theta)\,d\mathbf{x} \quad (2)$$

PLPDA antennas consist of several parameters such as dipole length, dipole spacing, and dipole width that determine the antenna's performance and overall size. PLPDA optimization begins by initially selecting a subset of these parameters that will be optimized for better performance and minimal antenna footprint. Each parameter chosen for optimization is subjected to an initial sampling strategy employing a normal distribution, characterized by a randomly selected mean value and an informed estimation of standard deviation. The use of a normal distribution for initial sampling is a common choice because it allows a diverse set of the initial candidate solutions that cover a wide range of the search space.

The antenna performance is evaluated for each candidate. After evaluating the performance of all candidates within the population, they are ranked to identify antennas with the smallest footprint and best gain and bandwidth performance. These top-ranking candidates are referred to as the elite set of candidates. These elite candidates will then determine the next normally distributed candidates. The process is repeated until the candidate population consists of optimized values. This process is illustrated in Fig. 2 [20].

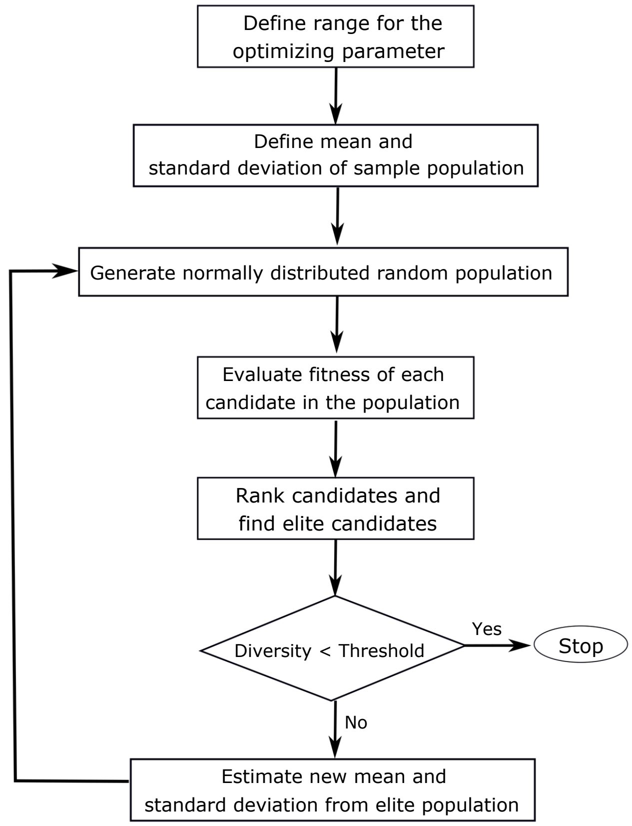

FIGURE 2. CE optimization flowchart [20].

3. PLPDA DESIGN

3.1. Reference PLPDA

An LPDA is composed of multiple dipoles whose dimensions and spacing are scaled by constant ratios to achieve broadband performance. In this configuration, L, D, and R represent the dipole length, diameter, and distance from the apex, respectively.

To establish a performance baseline, a reference PLPDA was designed using the standard LPDA synthesis method detailed in [24]. The target specifications were a bandwidth of 1.3–6.0 GHz and a directivity of 8.5 dB. From these parameters, the number of dipoles, their dimensions, and spacing factors were derived.

As in [22], the transition from a free-space LPDA to a printed configuration was performed by replacing cylindrical dipoles with stripline rectangular dipoles, whose equivalent widths w_n were obtained using

$$w_n = \pi a_n \quad (3)$$

The antenna was implemented on a Rogers RT 5880 substrate ($\epsilon_r = 2.2$, $h = 1.575$ mm), applying a scaling factor of

0.92 to account for the dielectric environment, as recommended in [25].

The resulting reference PLPDA measured 254.55 mm × 116.08 mm and was modeled in Computer Simulation Technology (CST) Design Studio. Its simulated bandwidth, gain, and radiation characteristics served as the baseline for the subsequent miniaturized designs presented in this study.

3.2. m-Segment PLPDA

To achieve lateral miniaturization, longer dipoles of the reference PLPDA were replaced with m-segment fractal dipoles following the procedure described in [22].

Figure 3 compares the longest dipole of the reference PLPDA with its m-segment equivalent, where (a) shows the reference dipole, and (b) shows the m-segment configuration. Although the total length of the individual segments is equal to that of the reference dipole, the effective span is reduced, leading to a narrower overall antenna profile.

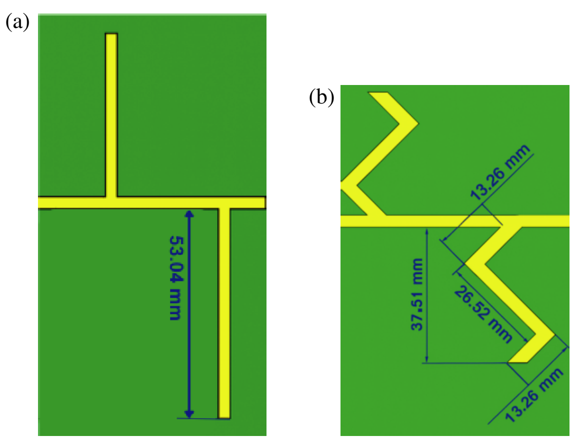

FIGURE 3. Comparison of reference and m-segment dimensions.

In this study, the previously validated configuration with $m = 2$ and $n = 1$ was adopted, as it demonstrated the most favorable balance between compactness and performance in [22]. As established in the earlier study, converting the two longest dipoles to m-segment geometry yielded optimal performance among several tested combinations. The resulting m-segment PLPDA achieved a width of 87.84 mm, corresponding to a 24.32% reduction relative to the reference design, while maintaining comparable S_{11} and gain characteristics (Fig. 4 and Fig. 5).

3.3. CE Optimized PLPDA

Building on the laterally miniaturized m-segment PLPDA, the next stage focused on axial length reduction using the CE optimization algorithm. The objective was to minimize the overall antenna profile while maintaining a wide impedance bandwidth and stable gain performance.

In a conventional PLPDA, the inter-element spacing (S_n) significantly contributes to the total axial dimension. These spacing values, initially derived from the standard PLPDA design equations (Table 1), were used as stochastic optimization

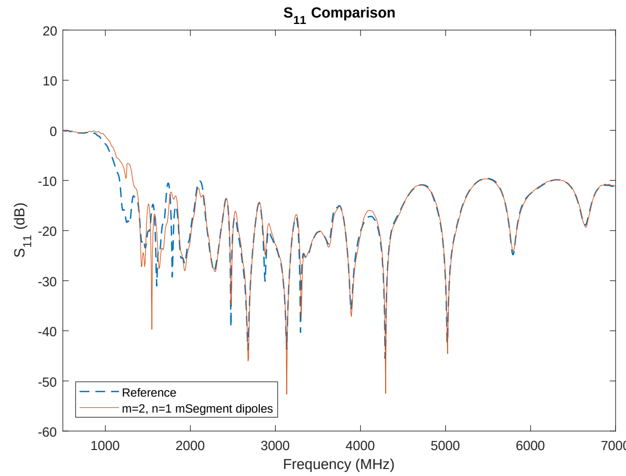

FIGURE 4. S_{11} comparison of reference and m-segment PLPDA.

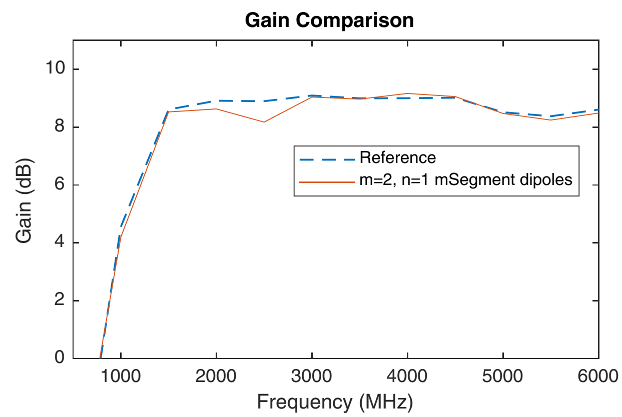

FIGURE 5. Gain comparison of reference and m-segment PLPDA.

parameters in the CE framework. Since shorter dipoles (elements 1–10) contribute minimally to the total length, optimization was applied only to dipoles 11–20, where spacing strongly influences axial size and phase alignment.

The selection of CE optimization for this application was motivated by several problem-specific considerations. The PLPDA spacing optimization involves a multi-dimensional parameter space (spacing values between dipole elements 11–20) with highly expensive objective function evaluations — each candidate antenna design requires a full-wave electromagnetic simulation in CST, with simulation times on the order of 30 minutes per design. With a population size of 20 candidates per generation, each optimization iteration requires approximately 10 hours of computational time. Under these constraints, the computational efficiency advantage of CE becomes critical. Based on the comparative data reported in [20], CE's reduction in required function evaluations (by a factor of approximately 6 relative to PSO for high-dimensional problems) translates directly to feasible optimization time scales.

Within this CE framework, each candidate antenna design was evaluated using a fitness function that balances three competing objectives: bandwidth coverage, gain performance, and axial compactness:

$$F = w_1 \cdot BW + w_2 \cdot G - w_3 \cdot L \tag{4}$$

where BW represents the bandwidth coverage metric defined as:

$$BW = \sum_{i=1}^{N} \delta_i, \quad \text{where} \quad \delta_i = \begin{cases} 1, & \text{if } S_{11}(f_i) < -10\,\text{dB} \\ 0, & \text{otherwise} \end{cases} \tag{5}$$

with N test frequencies distributed across the 1.3–6.0 GHz operating band to capture resonance behavior. G represents the average realized gain computed from multiple frequencies distributed across the operating band. L is the total axial antenna length (mm). All three objectives (BW, G, and L) were normalized using min-max normalization to ensure comparable scales before applying weights. The weighting factors $w_1 = 0.4$, $w_2 = 0.3$, and $w_3 = 0.3$ were selected to prioritize bandwidth preservation (highest weight) while treating gain and length reduction as equally important secondary objectives. This distribution ensures that candidates with high bandwidth coverage are systematically preferred while driving length reduction and maintaining acceptable gain levels.

Parameter bounds were defined as $\pm 50\%$ of the reference spacing values for dipoles 11–19, providing sufficient design space exploration while maintaining geometric feasibility.

The CE algorithm iteratively refined a multivariate normal sampling distribution $N(\boldsymbol{\mu}, \boldsymbol{\sigma}^2)$ for each spacing parameter. In each generation, 20 candidate designs were sampled from truncated normal distributions (bounded by the parameter limits), evaluated via CST simulation, and ranked by fitness. The top 2 candidates (elite ratio $\rho = 0.1$) were selected to update distribution parameters using exponential smoothing with $\alpha = 0.8$ for mean and dynamic smoothing for standard deviation ($\beta = 0.7$, modified by $\beta_{\text{mod}} = \beta - \beta(1 - 1/t)^q$ where t is the generation number and $q = 50$). Convergence was detected when $\max(\boldsymbol{\sigma}) \leq 10^{-6}$ mm or after 100 generations, whichever occurred first.

A MATLAB-CST co-simulation interface utilizing the CST COM API via MATLAB's actxserver functionality was employed for automated design evaluation. For each candidate, the algorithm updated the spacing parameters in the CST parametric model, executed the solver, extracted S-parameters at the test frequencies for bandwidth evaluation, retrieved 3D farfield patterns at multiple frequencies for gain evaluation, and calculated the total axial antenna length. The fitness score was then computed according to Eq. (4). This automated workflow enabled the complete optimization loop without manual intervention.

The CE algorithm ran for 7 generations until mathematical convergence ($\sim$ 140 evaluations, $\sim$ 70 hours total), with convergence detected when $\max(\boldsymbol{\sigma}) < 10^{-6}$ mm at generation 7. Early generations (1–3) explored the design space efficiently, while generations 4–5 progressively refined the search space. Generation 4 achieved the optimal balance: 100% bandwidth coverage with significant axial reduction (217 mm). Although later generations (6–7) achieved further length reduction to 203 mm, this came at the cost of bandwidth and gain degradation. The optimization exhibited stable behavior with no divergence throughout. Fig. 6 illustrates the evolution of antenna performance across seven CE optimization generations, highlighting the trade-off among axial length, bandwidth coverage, and average gain. A fourth-generation configuration provided the most balanced trade-off, achieving 100% bandwidth coverage, an axial length of 217 mm, and an average gain of 7.63 dB. This configuration (217 mm $\times$ 88 mm), highlighted in Fig. 6, was therefore selected as the optimized m-segment PLPDA.

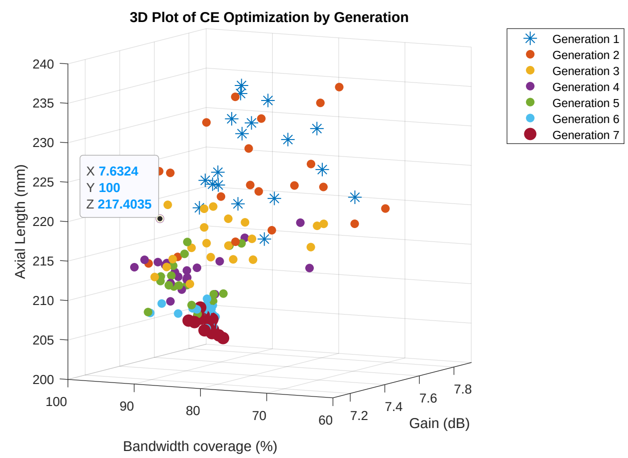

FIGURE 6. Evolution of axial length, gain, and bandwidth coverage during CE optimization. The highlighted point represents the final selected configuration.

The complete optimized antenna geometry is illustrated in Fig. 7, showing all 20 dipole elements with the feed point at the left end of the boom. The figure highlights the m-segment fractal geometry applied to dipoles 19 and 20, the optimized inter-element spacing values, and the overall compact dimensions of 217 mm $\times$ 88 mm. Key dimensional parameters are labeled: dipole lengths (l_n), dipole widths (w_n), and optimized spacing values (s_n). Complete dimensional data is provided in Table 1. The dipole length column includes m-segment effective lengths (for elements 19–20) shown in brackets and italic. Spacing is presented in two columns: conventional baseline values and CE-optimized values (italic). The antenna employs a microstrip feed with a transmission line width of 5.03 mm, providing a characteristic impedance of 50 Ω on the Rogers RT 5880 substrate ($h = 1.575$ mm, $\varepsilon_r = 2.2$).

4. RESULTS AND DISCUSSION

The performance of the optimized m-segment PLPDA was evaluated via both simulation and experimental measurements, and compared with those of the reference and the m-segment PLPDA. Key performance metrics, including impedance bandwidth, gain, and radiation characteristics, were analyzed to assess the effect of CE-based axial optimization.

The antenna prototype was fabricated on a Rogers RT 5880 substrate. The design accommodates standard PCB fabrication tolerances, with all feature sizes within standard manufacturing capabilities. The prototype was tested using a Vector Network Analyzer (VNA) and an anechoic chamber for performance validation. Fig. 8 illustrates the S_{11} and Fig. 9 depicts the far-field radiation and gain measurements at Laboratoire d'Electronique,

TABLE 1. Dimensions of optimized m-segment PLPDA.

n	Length (l_n) (mm)	Spacing (s_n) between n and $(n+1)$ (mm)		Width (w_n) (mm)
		Conventional	Optimized	
1	6.74	2.50	2.50	0.26
2	7.80	2.88	2.88	0.31
3	9.01	3.33	3.33	0.35
4	10.42	3.86	3.86	0.41
5	12.04	4.46	4.46	0.47
6	13.92	5.15	5.15	0.55
7	16.10	5.96	5.96	0.63
8	18.61	6.89	6.89	0.73
9	21.52	7.96	7.96	0.85
10	24.88	9.20	9.20	0.98
11	28.76	10.64	*8.61*	1.13
12	33.25	12.30	*9.67*	1.31
13	38.44	14.22	*12.48*	1.51
14	44.44	16.44	*13.11*	1.75
15	51.37	19.00	*14.63*	2.02
16	59.39	21.97	*21.27*	2.33
17	68.65	25.40	*22.79*	2.70
18	79.37	29.36	*24.99*	3.12
19	91.75 (*64.88*)	33.95	*28.53*	3.60
20	106.08 (*75.02*)			4.17

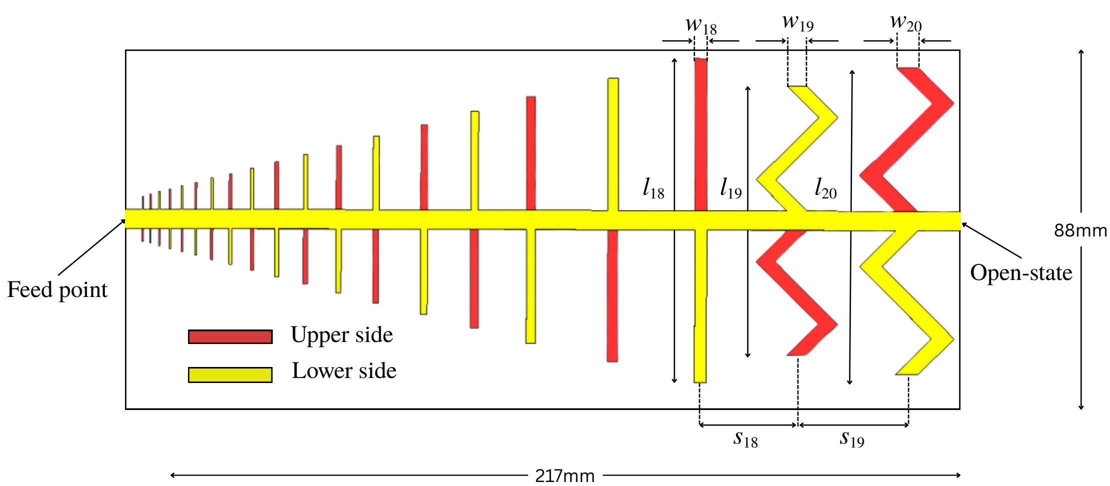

FIGURE 7. Complete geometry of the optimized m-segment PLPDA. Dimensional parameters are provided in Table 1.

Antennes et Telecommunications (LEAT), with the fabricated antenna mounted on the positioner.

The results for S_{11}, gain, and radiation patterns are illustrated in Figs. 11, 12, and 10, respectively.

The S_{11} response in Fig. 11 shows that the optimized m-segment PLPDA operates efficiently across the entire bandwidth range. Both simulated and measured results remained well below the -10 dB threshold, indicating excellent impedance matching and minimal reflection losses throughout the operating band. Minor variations between simulation and measurement are consistent with standard measurement uncertainties and typical tolerances in antenna fabrication and feed implementation, validating the antenna design.

The gain plot, illustrated in Fig. 12, shows a strong agreement between simulated and measured results of the optimized m-segment PLPDA. The gain remained consistently above 7 dB throughout the operating bandwidth, demonstrating robust performance across the frequency range.

In addition to the S_{11} and gain performance, the measured and simulated radiation characteristics of the optimized m-segment PLPDA were evaluated through the electric field horizontal (EH) and electric field vertical (EV) components at

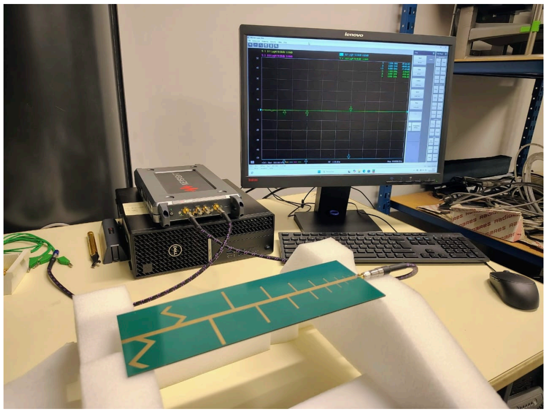

FIGURE 8. S_{11} measurement.

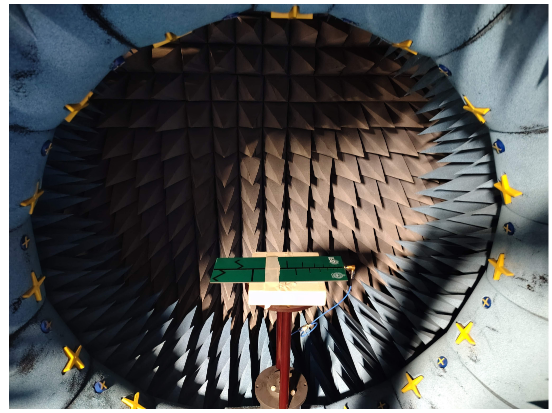

FIGURE 9. Gain measurement.

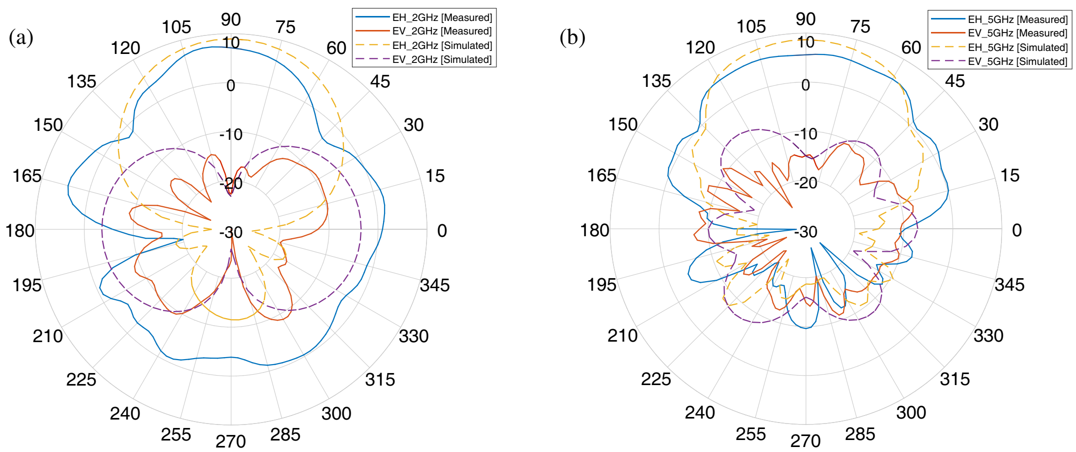

FIGURE 10. Radiation patterns of optimized m-segment PLPDA at (a) 2 GHz and (b) 5 GHz.

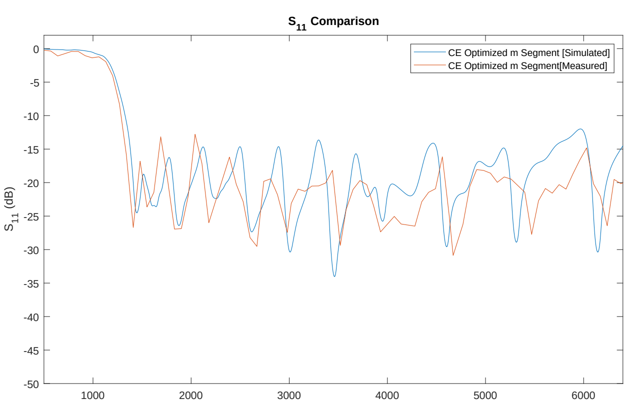

FIGURE 11. S_{11} comparison.

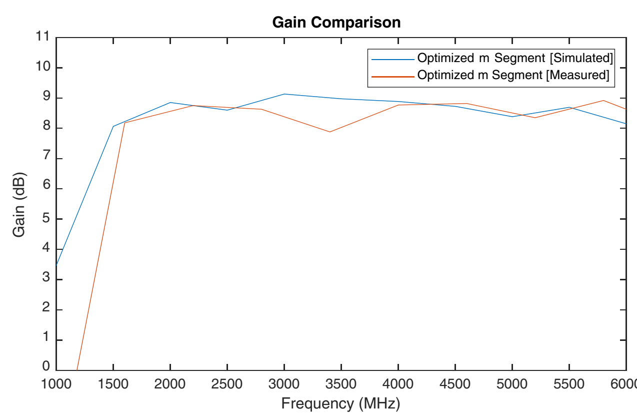

FIGURE 12. Gain comparison.

2 GHz and 5 GHz, as shown in Figs. 10(a) and (b), respectively. The results demonstrate a well-defined directional radiation behavior with a stable main-lobe orientation across the operating band. Good agreement between measured and simulated patterns was observed.

Quantitative analysis of radiation patterns confirms that the dual-dimensional miniaturization preserves directional characteristics. Front-to-back ratios exceed 20 dB across the operating band (20.5 dB at 2 GHz, 22.8 dB at 3 GHz, 28.3 dB at 5 GHz), validating the strong directivity observed in the pattern plots. Cross-polarization isolation exceeds 24 dB, demonstrating that the m-segment fractal geometry maintains polarization purity despite lateral compaction. These quantitative metrics, combined with the surface current analysis (Fig. 13) showing

TABLE 2. Comparison between the proposed PLPDA and previously reported designs.

Ref.	N	Bandwidth (GHz)	Gain (dB)	$L(\lambda) \times W(\lambda)$	Bandwidth Type	Gain Level
[26]	12	1.50–6.80	4.5–10.0	2.10×1.20	Wideband	Low-High
[27]	12	0.35–0.75	6.5–8.5	0.88×0.35	Narrowband	Moderate-High
[5]	50	0.55–9.00	2.4–7.8	0.49×0.36	Wideband	Low-High
[28]	16	0.87–7.42	1.2–3.0	0.45×0.29	Wideband	Low
[17]	25	0.50–10.00	3.0–6.1	0.36×0.43	Wideband	Low-Moderate
This work	20	1.30–6.00	7.8–9.4	0.94×0.38	Wideband	High

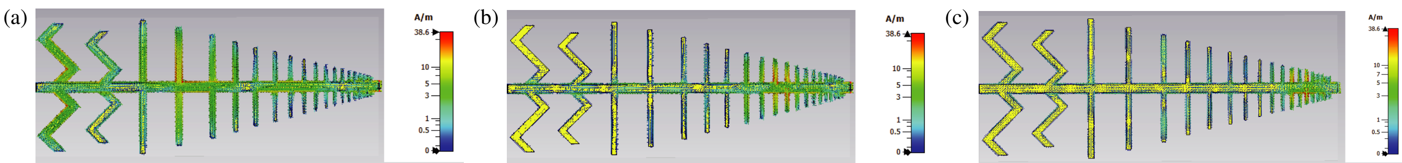

FIGURE 13. Surface current density distributions showing active region behavior at (a) 1.5 GHz, (b) 3.5 GHz, and (c) 6.0 GHz.

proper frequency-selective active region behavior, confirm that the footprint reduction does not introduce spurious coupling or current path disruptions.

Compared to the reference PLPDA baseline (254.55 mm $\times$ 116.08 mm), the optimized design achieves 34% footprint reduction (217 mm $\times$ 88 mm) while maintaining excellent gain (7.8–9.4 dB) and identical bandwidth coverage (1.3–6.0 GHz). This demonstrates effective miniaturization without performance degradation.

The proposed antenna design in this study demonstrates significant advancements compared with existing designs, as summarized in Table 2. It should be noted that the dimensions of the LPDAs in Table 2 are expressed in terms of the maximum wavelength within their operating frequency bands. In addition to the conventional parameters, the reported antennas were categorized according to bandwidth type and gain level to better highlight the practical performance trade-offs. Antennas covering more than a $3:1$ frequency ratio are classified as wideband, while gain levels are categorized as low (< 5 dB), moderate (5–7 dB), and high (> 7 dB).

As observed in Table 2, the proposed design maintains a consistently high gain (> 7 dB) across the entire operating band (1.30–6.00 GHz, $4.6 : 1$ ratio) and is therefore classified as both wideband and high gain. In contrast, several referenced works exhibit gain ranges spaning from low to high, despite wideband operation. For example, [26] and [5] demonstrate wideband performance; however, their gain levels vary significantly across the band, covering low-to-high classifications. Moreover, [26] employs substantially larger electrical dimensions, and [5] requires a considerably higher number of dipole elements (50 elements). Some antennas achieve moderate-to-high gain but operate in narrowband regimes (e.g., [27]), whereas others provide wideband performance with low or low-to-moderate gain levels ([17, 28]). With 20 dipole elements, the proposed design achieves an effective balance between structural complexity and performance, avoiding an excessive element count while delivering stable, high gain throughout the entire bandwidth.

In terms of electrical size, the axial length of 0.94λ and lateral width of 0.38λ represent a substantial footprint reduction compared with conventional implementations. The axial length of 0.94λ, achieved through cross-entropy optimization by reducing the spacing between dipoles, compares favorably with references such as [26] and [27], and [26] is significantly larger than the proposed design. The lateral length of 0.38λ, minimized using m-segment optimization, is comparable to [27] and [5], and smaller than [26].

Refs. [28] and [17] present smaller overall electrical dimensions; however, an examination of their qualitative performance classifications reveals important trade-offs. Ref. [28] achieves wideband operation but with a low gain level (1.2–3.0 dB), which is more than 6 dB lower than the proposed design across the operating band. Ref. [17] achieves wideband operation but with a low-to-moderate gain level (3.0–6.1 dB) using dual-band dipoles with top loading. In contrast, the proposed design achieves wideband operation with a consistently high gain. Furthermore, Refs. [28] and [17] employ dual-band dipoles and bow-tie-shaped dipoles with top loading, respectively, to achieve their compact size. In contrast, our design uses an m-segment fractal structure and dipole spacing reduction to achieve compactness without significantly altering the fundamental dipole shape, which simplifies the design and potentially enhances manufacturability and robustness.

The achieved miniaturization while maintaining wideband performance is enabled by complementary electromagnetic mechanisms. The m-segment fractal geometry achieves lateral compaction through its space-filling property: extended conductor length is curled within a finite volume [16], with total geometrical length preserved as $L(\sqrt{2})^n$ [16]. This maintains designed resonant frequencies despite physical compaction. The fractal's symmetry around the dipole axis preserves undistorted radiation patterns [16]. The CE-optimized spacing achieves axial compaction while maintaining LPDA phase progression and active region behavior essential for wideband operation. Surface current distributions (Fig. 13) validate this mechanism: at lower frequencies, current concentrates on the longer m-segment dipoles, while at higher frequencies, the active region shifts to the shorter elements, confirming proper frequency-selective operation. The multi-objective fitness function (Eq. (4)) inherently penalizes bandwidth degradation, exploring only viable configurations. These mechanisms — lateral and axial reduction on orthogonal dimensions — achieve 34% footprint reduction while preserving measured $S_{11} < -10$ dB across 1.3–6.0 GHz with 7.8–9.4 dB gain.

The 34% reduction represents an optimized balance rather than a fundamental limit. As shown in Fig. 6, generation 7 achieved 203 mm axial length compared to the selected 217 mm, but degraded bandwidth and gain. Further spacing reduction violates LPDA phase progression and active region requirements, increasing mutual coupling. The lateral miniaturization via m-segment fractal geometry is similarly constrained. Increasing the m-segment iteration number or applying the fractal to additional dipoles would further reduce lateral dimensions but at the cost of increased fabrication complexity (finer features) and potential degradation of current-distribution continuity. The selected configuration ($m = 2$, $n = 1$, applied to dipoles 19–20) represents an optimal balance. The 34% reduction prioritizes robust wideband performance over aggressive compaction.

The compact size, combined with high gain and adequate bandwidth, justifies the efficacy and superiority of this design. These attributes collectively provide a robust solution, demonstrating that the compact dimensions do not detract from the antenna's high performance, making it suitable for applications where space is limited yet high performance is essential.

5. CONCLUSION

This study presents the design and experimental validation of a miniaturized single-layer PLPDA antenna operating from 1.3–6.0 GHz. The antenna was developed through a sequential miniaturization process involving m-segment fractal geometry for lateral size reduction and CE optimization for axial length reduction.

The application of m-segment geometry reduced the antenna width by 24%, while CE optimization further reduced the axial dimension by 15%. The resulting antenna achieved an overall footprint reduction of 34% (217 mm × 88 mm) compared with the reference design.

The experimental measurements were closely aligned with the simulation results, validating the effectiveness of the proposed optimization framework. The measured S_{11} remained well below -10 dB across the entire operating band, and the average measured gain exceeded 7 dB, confirming strong impedance matching and stable radiation characteristics.

The results demonstrate that CE optimization serves as an effective tool for adaptive axial miniaturization, enabling performance-aware tuning of structural parameters beyond the analytical limits. Combined with the m-segment fractal approach, it provides a practical and scalable pathway for developing compact wideband LPDA antennas. The compact form factor and wideband coverage make the design suitable for spectrum monitoring, IoT gateway receivers, and software-defined radio platforms where size, multi-band operation, and directional characteristics are essential.

ACKNOWLEDGEMENT

This work was partially funded by the Indo-Sri Lanka Joint Research Programme 2019.

This work was also supported by a short-term scientific stay scholarship from the French Government through the Embassy of France to Sri Lanka and Maldives.

REFERENCES

[1] Rostami Gooran, P., A. Lalbakhsh, H. Moradi, and M. Jamshidi, "Compact and wideband printed log-periodic dipole array antenna using multi-sigma and multi-Tau techniques," *Journal of Electromagnetic Waves and Applications*, Vol. 33, No. 6, 697–706, 2019.

[2] Mistry, K. K., P. I. Lazaridis, Z. D. Zaharis, and T. H. Loh, "Design and optimization of compact printed log-periodic dipole array antennas with extended low-frequency response," *Electronics*, Vol. 10, No. 17, 2044, 2021.

[3] Abdulhameed, A. A. and Z. Kubík, "Design a compact printed log-periodic biconical dipole array antenna for EMC measurements," *Electronics*, Vol. 11, No. 18, 2877, 2022.

[4] Ibrahim, I. M., M. I. Ahmed, H. M. Abdelkader, and M. M. Elsherbini, "A novel compact high gain wide-band log periodic dipole array antenna for wireless communication systems," *Journal of Infrared, Millimeter, and Terahertz Waves*, Vol. 43, No. 11, 872–894, 2022.

[5] Kyei, A., D.-U. Sim, and Y.-B. Jung, "Compact log-periodic dipole array antenna with bandwidth-enhancement techniques for the low frequency band," *IET Microwaves, Antennas & Propagation*, Vol. 11, No. 5, 711–717, 2017.

[6] Sun, Q., J. Wang, J. Cui, J. Fu, C. Zhou, and E. Wang, "A compact printed log-periodic antenna with loaded stub," in *Proceedings of 2014 3rd Asia-Pacific Conference on Antennas and Propagation*, 593–595, Harbin, China, 2014.

[7] Chen, J., J. Ludwig, and S. Lim, "Design of a compact log-periodic dipole array using T-shaped top loadings," *IEEE Antennas and Wireless Propagation Letters*, Vol. 16, 1585–1588, 2017.

[8] Park, J., C. Im, and H. Choo, "Design of a Koch-curved LPDA antenna with optimized beamwidth to improve the aperture efficiency of reflector antennas," *IEEE Access*, Vol. 13, 106 747–106 758, 2025.

[9] Rajendran, J. and S. K. Menon, "A low-cost compact wideband printed planar log periodic sierpinski antenna," in *2016 Progress in Electromagnetic Research Symposium (PIERS)*, 2752–2756, Shanghai, China, Aug. 2016.

[10] Oraizi, H., A. Amini, and M. K. Mehr, "Design of miniaturised UWB log-periodic end-fire antenna using several fractals with WLAN band-rejection," *IET Microwaves, Antennas & Propagation*, Vol. 11, No. 2, 193–202, 2017.

[11] Li, D. and J.-F. Mao, "Sierpinskized Koch-like sided multifractal dipole antenna," *Progress In Electromagnetics Research*, Vol. 130, 207–224, 2012.

[12] Karmakar, A., "Fractal antennas and arrays: A review and recent developments," *International Journal of Microwave and Wireless Technologies*, Vol. 13, No. 2, 173–197, 2021.

[13] Jena, M. R., S. Sahoo, G. P. Mishra, and B. B. Mangaraj, "Miniaturised band notched printed LPDA design with meander fractal dipole for UWB communication," *International Journal of Electronics*, Vol. 108, No. 1, 21–44, 2021.

[14] Xiong, Y. and B. Zhang, "A miniaturized three-dimensional log periodic Koch-dipole array antenna using T-shaped top loading," *International Journal of RF and Microwave Computer-Aided Engineering*, Vol. 31, No. 7, e22678, 2021.

[15] Rosmin, M. H., M. K. A. Rahim, N. S. Yaziz, M. N. Iqbal, O. Ayop, and M. A. H. Kamarusshahrin, "Second iteration of slotted fractal log periodic dipole antenna for UHF digital TV band application," *ELEKTRIKA — Journal of Electrical Engineering*, Vol. 20, No. 3, 48–52, 2021.

[16] Khokle, R. P., "Generation, application and analysis of a novel family of m-segment quadratic fractal curves to antennas," *Progress In Electromagnetics Research C*, Vol. 65, 191–200, 2016.

[17] Anim, K. and Y.-B. Jung, "Shortened log-periodic dipole antenna using printed dual-band dipole elements," *IEEE Transactions on Antennas and Propagation*, Vol. 66, No. 12, 6762–6771, 2018.

[18] Pu, J. and B. Zhang, "Redundancy elimination of the classic log-periodic dipole array antenna by resonance point optimization for a miniaturized structure," *IEEE Transactions on Antennas and Propagation*, Vol. 69, No. 12, 8345–8353, 2021.

[19] Gajbhiye, P. A., S. P. Singh, and M. K. Sharma, "A comprehensive review of AI and machine learning techniques in antenna design optimization and measurement," *Discover Electronics*, Vol. 2, No. 1, 46, 2025.

[20] Kovaleva, M., D. Bulger, B. A. Zeb, and K. P. Esselle, "Cross-entropy method for electromagnetic optimization with constraints and mixed variables," *IEEE Transactions on Antennas and Propagation*, Vol. 65, No. 10, 5532–5540, 2017.

[21] Rubinstein, R. Y., "Optimization of computer simulation models with rare events," *European Journal of Operational Research*, Vol. 99, No. 1, 89–112, 1997.

[22] Herath, H. M. S. M., J. M. J. W. Jayasinghe, and D. N. Uduwawala, "M-segment printed log periodic dipole array antennas," in *2023 IEEE 17th International Conference on Industrial and Information Systems (ICIIS)*, 97–102, Peradeniya, Sri Lanka, 2023.

[23] Botev, Z. I., D. P. Kroese, R. Y. Rubinstein, and P. L'ecuyer, "The cross-entropy method for optimization," in *Handbook of statistics*, Vol. 31, 35–59, 2013.

[24] Balanis, C. A., *Antenna Theory: Analysis and Design*, John Wiley & Sons, 2015.

[25] Pantoja, R., A. Sapienza, and F. M. Filho, "A microwave printed planar log-periodic dipole array antenna," *IEEE Transactions on Antennas and Propagation*, Vol. 35, No. 10, 1176–1178, 1987.

[26] Hu, Z., Z. Shen, W. Wu, and J. Lu, "Low-profile log-periodic monopole array," *IEEE Transactions on Antennas and Propagation*, Vol. 63, No. 12, 5484–5491, 2015.

[27] Bishop, N. A., J. Miller, D. Zeppettella, W. Baron, J. Tuss, and M. Ali, "A broadband high-gain bi-layer LPDA for UHF conformal load-bearing antenna structures (CLASs) applications," *IEEE Transactions on Antennas and Propagation*, Vol. 63, No. 5, 2359–2364, 2015.

[28] Yeo, J. and J.-I. Lee, "Miniaturized LPDA antenna for portable direction finding applications," *ETRI journal*, Vol. 34, No. 1, 118–121, 2012.